Superconductivity 7 (2023) 100058

Contents lists available at ScienceDirect

Superconductivity

journal homepage: www.elsevier.com/locate/supcon

Full Length Article

Magnetic bearings with double crossed loops modelled with T-A formulation and electric circuits

Bárbara Maria Oliveira Santos [a,*], Gabriel dos Santos [a], Flávio Goulart dos Reis Martins [b], Felipe Sass [b], Guilherme Gonçalves Sotelo [b], Rubens de Andrade Junior [c], Francesco Grilli [d]

[a] Electrical Engineering Department, Rio de Janeiro State University, Rio de Janeiro, 20550-900, Rio de Janeiro, Brazil
[b] Electrical Engineering Department, Universidade Federal Fluminense, Niterói, 24210-240, Rio de Janeiro, Brazil
[c] Electrical Engineering Department, Universidade Federal do Rio de Janeiro, Rio de Janeiro, 21941-909, Rio de Janeiro, Brazil
[d] Institute for Technical Physics, Karlsruhe Institute of Technology, Karlsruhe, 76131, Germany

ARTICLE INFO

Keywords:
Coated conductors
Jointless loops
T-A formulation

ABSTRACT

The application of High-Temperature Superconductor (HTS) coils made of coated conductors has been investigated for many years. A possible configuration for such coils is the jointless loop, also known as the ring coil. The double crossed loop coil (DCLC) has been successfully applied in superconducting magnetic bearings (SMBs). The design of SMBs with DCLCs requires flexible modelling to allow all parts of the device to be represented. This work proposes the T-A formulation with a thin-film approximation for modelling SMB with DCLCs in the finite element analysis framework. A 2D representation of the system is coupled with an external electric circuit to model the continuity of the lines that represent the parts of each jointless loop. To couple the T-A formulation and the circuit, an average of the total electric field, with both resistive and inductive components, is applied to the circuit. The total current computed by the circuit is applied to the T-A formulation. The proposed methodology was validated by comparison with levitation force experimental data. Two types of tests were simulated: five levitation force tests and three guidance force tests. It is shown that there is a limit to the behaviour of the levitation force related to the high-loss state. Below this limit, the stack of DCLCs behaves as an equivalent bulk. Beyond this limit, a high-loss state appears as a linear growth of the levitation force. It is also shown that this high-loss state in vertical displacement influences the lateral force.

1. Introduction

Jointless loops of coated conductors have been proposed as a way to trap more magnetic fields and to lower losses and hot spots in HTS coils. Electric machinery [1] and magnetic bearings [2] are among the applications proposed for this type of coils.

The geometry of jointless loops has been investigated in several configurations, such as the single current loop coil [3], the two current loops coil [4], and the double crossed loop coil (DCLC) [2], which includes two intertwined single current loops. This configuration aims to correct the asymmetry of the single current loop and to increase the amount of superconducting material occupying the same volume [2]. Fig. 1 shows two illustrations of the DCLC over a magnetic guideway: a 3D illustration and its 2D approximation.

The current continuity between parts of the same single loop in a 2D approximation is asymmetrical and, therefore, cannot be correctly represented by simple homogenization in finite element models. The thin-film approximation is an efficient way to describe the loops in 2D. This has been done with the Integral Equations Method (IEM) [5] to investigate the behaviour of the superconducting magnetic bearing with double crossed loops. One is illustrated in Fig. 1. This model included two sets of double crossed loops with 50 tape segments each and the magnetic guideway in a Halbach configuration with Nd-Fe-B permanent magnets and electrical steel pieces as flux concentrators. Two further approximations were made to reduce the computational complexity of the IEM. The first one was that the double crossed loops and the guideway were simulated separately, and the magnetic field produced by the guideway was entered as a source of the simulations of the loops. The second one was that only one set of double crossed loops was represented, as the magnetic field symmetry was considered a boundary condition. These approximations reduced the applicability of the model to different and more complex scenarios.

Another electromagnetic modelling option for this type of bearing is the T-A formulation [6]. Solely based on differential equations, it is more practical than the IEM because it allows the inclusion of both guideway and coated conductors in the same computational model.

* Corresponding author.
E-mail address: barbara.santos@eng.uerj.br (B.M.O. Santos).

https://doi.org/10.1016/j.supcon.2023.100058
Available online 8 August 20232772-8307/

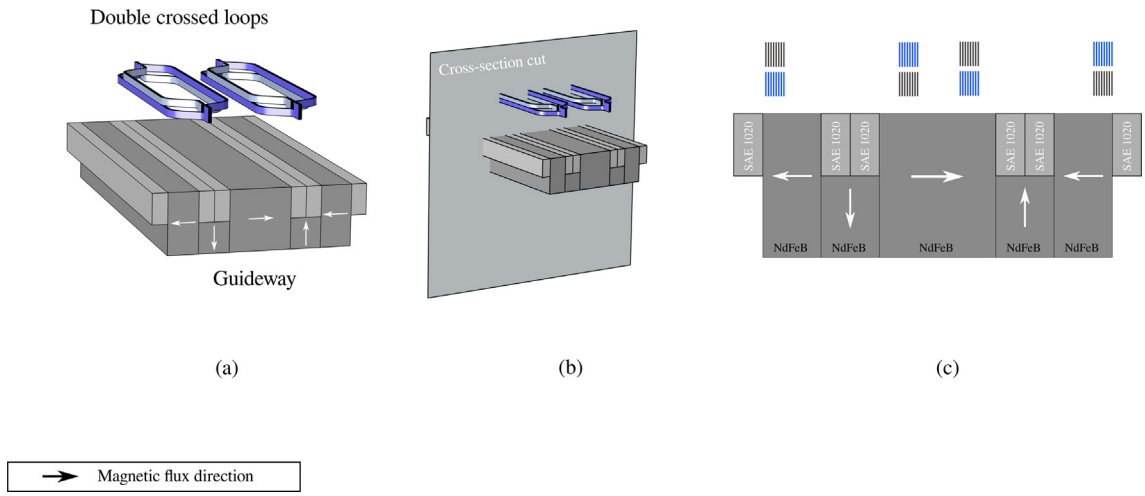

Fig. 1. Illustration of two sets of double crossed loops over the magnetic guideway. The main magnetization direction of the magnets is represented with white arrows. (a) is the 3D representation of the system while (b) is the chosen cross-section to apply the 2D approximation and (c) is its 2D approximation. Each loop becomes a line in a 2D approximation. Blue and gray colors represent the loops' overall continuity.

It uses the A formulation to represent the magnetic field in all finite element domains, making it simple to configure the non-linear models for the permanent magnets and the ferromagnetic materials, as well as a moving mesh to represent the movement between the guideway and the superconductors.

With the T-A formulation, several options for modelling the current continuity between tape segments have been proposed in the literature, such as the connection of points with virtual lines [7], the application of Neumann conditions along with integral restrictions [8], and the use of an auxiliary circuit [9,10]. The auxiliary circuit method is the method chosen for this work.

In this work, we present the application of the T-A formulation with an auxiliary circuit to model a superconducting magnetic bearing with double crossed loop coils. We prove that the T-A formulation with auxiliary circuits is an efficient choice to represent the current continuity problem posed by the 2D approximation of double crossed loops. The computational model is validated with measurements of levitation force published in [5]. Then, several levitation force tests are simulated, compared and their hysteresis behaviours are analysed. Guidance force tests are also simulated and the guidance force behaviour of the magnetic bearing with double crossed loops is analysed. To the best of our knowledge, no other work has investigated the guidance force of superconducting magnetic bearings with double crossed loops so far, with neither simulations nor experimental work. So, this work also presents the first investigations of the current induction dynamics of double crossed loops with lateral displacement. These investigations are important for the development of this type of superconducting magnetic bearings, which is highly dependent on force hysteresis.

This paper is divided into five sections. Section 2 discusses the computational model: the magnetic bearing and the T-A formulation with an auxiliary circuit. Section 3 details the methodology, with descriptions of how the computational model was implemented and of the levitation and guidance force tests. Section 4 presents the results and discussions and Section 5 summarizes the conclusions.

2. Coupling double crossed loop coils in 2D with T-A formulation

In this section, the computational model is described. First, there is a brief explanation of the magnetic bearing with DCLC. Then, the application of the T-A formulation with an auxiliary circuit to this type of magnetic bearings is detailed.

2.1. Magnetic bearing with double crossed loop coils

The magnetic bearing with DCLC is composed of: a magnetic guideway with permanent magnets (and, if necessary, soft ferromagnetic materials acting as flux concentrators) and of double crossed loops of coated conductors. This type of bearing was proposed in [2] and was based on the single loop behaviour investigated in [11]. Compared to bulk superconductors and a stack of coated conductors, the single loop has the best force per volume ratio [11] because it uses much less superconducting material than bulks and allows larger current paths than those found in stacks, which are limited by their width, for example, 4 mm, 6 mm and 12 mm.

During operation as a bearing, the cooling process and the movement between the guideway and the DCLCs induce a current in the loops. The induced current may have a persistent nature, sustaining both levitation force and guidance force. Levitation force experiments were performed both on single and double crossed loops in previous works [11,5]. In this type of experiment, the vertical distance between the guideway and the loops is first decreased and then increased, and the levitation force is measured. It was found that the levitation force behaviour of both single [11] and double crossed loops [2] changes during the first part of the experiment when the vertical distance decreases. The levitation force has a non-linear behaviour, similar to what is observed in bearings with bulks [12], up to a certain vertical position. Then, the overall behaviour changes to approximately linear, which causes the loops to have higher hysteresis in their levitation force response if compared to both bulks and stacks of coated conductors. This phenomenon is analyzed in this work.

Each double crossed loop has an asymmetrical current continuity, as shown in Fig. 1. The continuity is set tape by tape, with two tapes per double crossed loop. So, any simulation work designed to model the behaviour of these bearings needs to consider this continuity. Reference [5] proved that, because of this type of continuity, the stacks of double crossed loops cannot be modeled by the common homogenization method. As it needs to be tape-by-tape, an appropriate approach is to apply a thin-film approximation. A suitable modelling option is the integral equations method (IEM).

A simulation model including the IEM was developed in [5] and applied to model the levitation force experiments. A good agreement between simulations and measurements was obtained. However, the IEM computational model proved to be too costly in terms of memory occupation and computation time. Due to these constraints, a decoupled approach was chosen, in which the guideway and the DCLCs were

simulated separately. First, the guideway was simulated alone with its movement for the evaluation of the magnetic field distribution in space and time. Then, the magnetic field for each time step was applied as a source at the boundaries of the IEM simulation of the DCLCs. Although such decoupling decreases the computation time considerably, it forces the disregarding of the counter-magnetomotive force due to the induced currents at the close vicinity of the DCLCs and its possible demagnetizing effects on the guideway magnets. Also, domain reductions were applied with the use of boundary conditions. A more general computational approach is necessary to allow the magnetic bearings with double crossed loops to be designed and investigated in various operational conditions.

2.2. T-A formulation with an auxiliary circuit

The T-A formulation [6] is a good option to model the behaviour of magnetic bearings with DCLCs. First, it allows using the thin-film approximation, which is the most appropriate choice to represent the coated conductors arranged as asymmetrical intertwined loops. Second, it is only based on differential equations, with the A-formulation part computing the magnetic vector potential, **A**, and the magnetic flux density, **B**,

$$\nabla \times \frac{1}{\mu} \nabla \times \mathbf{A} = \mathbf{J}, \tag{1}$$

$$\nabla \times \mathbf{A} = \mathbf{B}, \tag{2}$$

with μ as the magnetic permeability and **J** as the current density, while the T-formulation part computes the current vector potential, **T**, and the current density, **J**.

$$\nabla \times \rho \nabla \times \mathbf{T} = -\frac{\partial \mathbf{B}}{\partial t}, \tag{3}$$

$$\nabla \times \mathbf{T} = \mathbf{J}. \tag{4}$$

with ρ as the resistivity.

The A-formulation equations are applied to all the domains. Since it is a well-established way to model electric equipment, the methods to reproduce the behaviour of permanent magnets, ferromagnetic materials and mesh movement are well known and easy to use. Therefore, it is feasible to build a totally coupled simulation in which both guideway and permanent magnets are modelled together. This potential of the T-A formulation has been shown also for the simulation of superconducting electrical machines [13].

As for the T-formulation, it is only computed in the superconducting domains and its main goal is to correctly calculate the current density distribution in the superconductors. In 2D simulations, such as the ones presented and examined in this work, there is a necessity to apply other computational methods to couple two parts of the same tape, as shown in Fig. 2. Several methods of current sharing coupling have been explored in the literature.

The auxiliary circuit method developed in [9] and applied in [10], makes use of an auxiliary circuit to model the current sharing problem. This is done by representing the coated conductors as circuit elements, both by considering the non-linear resistivity, calculating the inductance and including them in the circuit [9], or by entering the more general equation [10],

$$v_{HTS} = \text{average}\left(\rho \mathbf{J} + \frac{\partial \mathbf{A}}{\partial t}\right) L. \tag{5}$$

The average operator is applied to the coated conductor's width so the electric potential, which is defined node by node in the 2D or 3D finite element mesh, can be used in the circuit. The current computed by the circuit is applied to the T formulation as a Dirichlet Boundary Condition. L is the active length of the coated conductor segment.

Fig. 2 shows how a single loop is included in the circuit. Each loop becomes two partial tape segments with half the width in the 2D approximation. For each segment, the average potential difference is computed and included in the circuit between two nodes. One of them is the calculated potential difference, and the other is the ground. The circuit simulator attached to the finite element software then computes the resulting current.

3. Methodology

In this section, the methodology applied in this work is described. First, the overall modelling of the coated conductors is discussed, followed by the description of the considered characteristics and parameters of the other materials involved, namely the permanent magnets and ferromagnetic flux concentrators. Then, the performed simulations are described. All simulations were performed with COMSOL Multiphysics 6.0, with the A-formulation applied with the Magnetic Field physics, the T-formulation applied with the Boundary PDE physics and the circuit applied with the Electric Circuits physics.

Two macro regions are created to configure the moving mesh: a stationary region, where there is air and the superconductors; and a deforming region, where the magnetic guideway and air are. This is chosen to avoid numerical errors that could occur by applying a moving mesh to the superconductor. COMSOL's Moving Mesh feature is used to model the movement. In the deforming region, movement is applied to the magnetic guideway domains by inserting the deforming equations. A linear equation is applied for levitation force simulation, going upward until needed and then downward. For the simulations of the guidance force, linear equations for both vertical and lateral movement are applied. The Moving Mesh feature uses smoothing equations for the mesh movement. This work applies a Laplace equation with the x and y positions as variables. During the simulation, the mesh is rebuilt several times to achieve better accuracy.

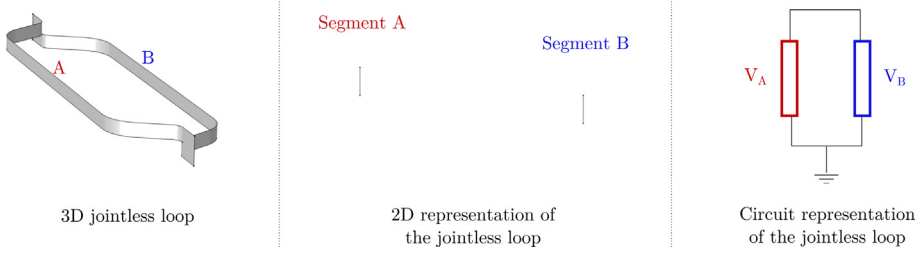

Fig. 2. Three representations of one jointless loop. 3D, the 2D approximation and the equivalent circuit. 2D and the circuit are used to represent the 3D model.

3.1. Materials properties

In this work, the coated conductors are considered as thin films characterised by a non-linear resistivity,

$$\rho = \frac{E_c}{J_c}\left|\frac{J_z}{J_c}\right|^{n-1}, \tag{6}$$

where E_c as the critical electric field, used commonly in the literature as 1μV/cm, J_z is the current density in the $\hat{z}$ direction, which is normal to the 2D $\hat{x}-\hat{y}$ plane represented in the simulations, and n is the power-law index, set to 20. J_c is the critical current density, which in this work is considered to be dependent on the magnetic field. It is computed by the elliptical equation,

$$J_c = \frac{J_{c0}}{\left(1+\frac{\sqrt{(kB_{\parallel})^2+B_{\perp}^2}}{B_0}\right)^b}, \tag{7}$$

with J_{c0}, k, b, B_0 as fit parameters set according to the experimental data available, with J_{c0} set as 2.2×10^{10} Am^{-2}, k is equal to 0.6, $B_{\parallel}$ the magnetic induction parallel to the tapes' surface, $B_{\perp}$ the magnetic induction normal to the tapes' surface, B_0 is set as 0.015 T, and b is set as 0.37. These parameters were chosen from [5], except for J_{c0}, which was adjusted according to the levitation force experimental data.

Three other materials are represented in the simulations: air, NdFeB permanent magnets and SAE 1020 carbon steel. The air is considered non-conducting, with null conductivity and permeability equal to the permeability of the vacuum. The NdFeB permanent magnets are modelled with the remanent induction method, and the SAE 1020 carbon steel pieces are modelled with their B-H curve. The parameters for these materials are summarized in Table 1. The simulated geometry is exactly the same as the one described in [5].

3.2. Simulations of the levitation force experiment

In these simulations, the goals are to compute the levitation force between double crossed loops and the guideway for various vertical displacements and to observe the current density normalised by the critical current density in each tape at many time instants. This is done for the simulation of the largest vertical displacement, which is the most extreme situation in terms of losses. These analyses are to help in the investigation of the behaviour of the levitation force with increasing displacements, or, better yet, with increasing losses. This information is of extreme importance for the design of magnetic bearings as the loss of levitation force may impair the bearing's functionality.

For all cases, at the beginning of the simulation, there is a 50 mm air gap between the guideway and the DCLCs. Then, the guideway is set to move with 1 mm/s speed, first upward and then downward, according to the vertical displacement chosen. Five cases are studied, with five different vertical displacements: ±10 mm, ±15 mm, ±20 mm, ±25 mm and ±30 mm. The last case, ±30 mm, is the one used for validation of the simulations by comparison to the experimental data available from [5].

Movement is implemented with a moving mesh setup, by which the guideway mesh is distorted in accordance with the movement. The mesh is rebuilt every 5 s to ensure that the element quality is maintained. Fig. 3 shows the simulated system of the ±30 mm case at two instants, along with the magnetic induction and flux lines. The first, Fig. 3a, shows the system at 0 s, where the guideway and the DCLCs are 50 mm apart. The box line surrounding the guideway is defined to separate the DCLCs and their surrounding air meshes from the guideway and its surrounding air mesh, which is distorted by movement. Fig. 3b shows the 30 s instant, where the DCLCs and the guideway are 20 mm apart.

The force is computed as

$$F_y = \gamma \int_C B_x J_z L dC \tag{8}$$

where B_x is the magnetic induction component in the $\hat{x}$ direction, C are the coated conductor segments, L is the straight part of the loops, set to 100 mm, and γ is the 2D approximation factor. The need for this factor was discussed in [5] and is related to the coil heads' contribution to the levitation force, only observable in 3D models. This points out the possibility of a definition of an adequate length computing the contributions of both the straight parts and the coil heads without the need for nonlinear adjustments, which would be highly dependent on the

Table 1
Parameters of the permanent magnets and the carbon steel pieces.

Parameters	Values
$\mathbf{B}_r$ - magnet	1.1 T
μ - magnet	μ_0
σ - magnet	7.14×10^5 S/m
σ - steel	8.41×10^6 S/m
$\mathbf{B}_{sat}$ - steel	1 T

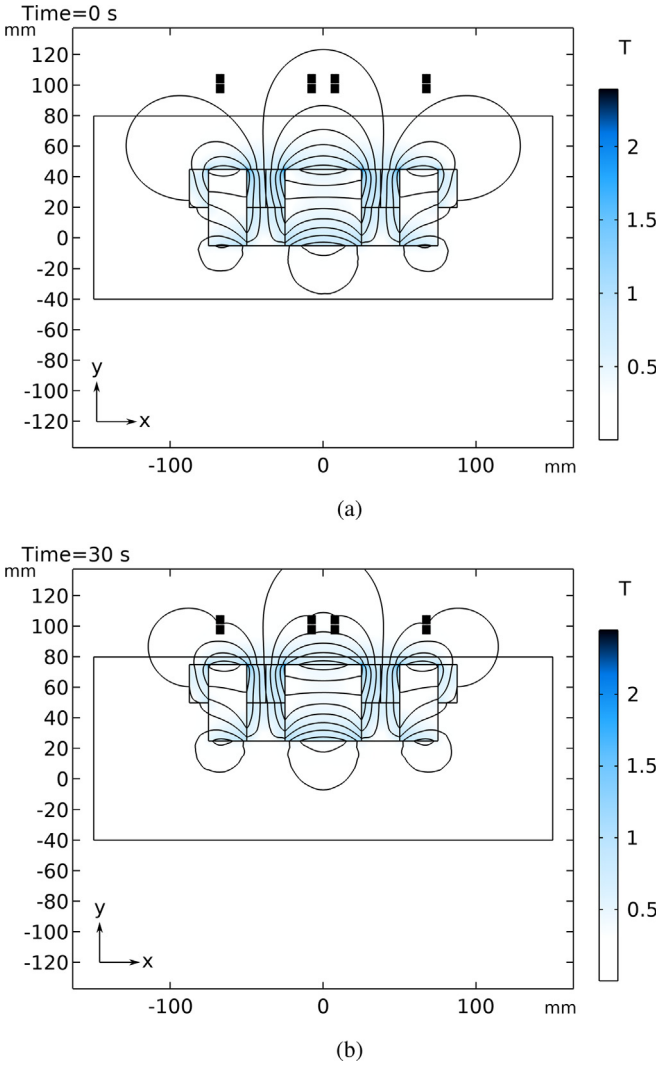

Fig. 3. Magnetic flux density magnitude and direction (represented by lines) at (a) 0 s and (b) 30 s. The part modelled with moving mesh is inside the inner rectangle. The guideway moves upwards, as it is shown in the figure, and then downwards, returning to its first position.

electromagnetic conditions of the coil (for example, if the coil heads had a high influence on the force density, the constant adjustment would fit for one part of the levitation curve, but not for the entirety of it, as very different electromagnetic conditions happen throughout the experiment). In this work, γ is set to 1.4 to match the $\pm$30 mm experimental data. It is a little lower than the one found in [5], 1.67, but it is of the same order of magnitude. The degrees of freedom (DoF) are counted as: 79183 DoF for $\mathbf{A}$, 6200 for $\mathbf{T}$, 100 for current computation and 2732 for the mesh displacement, totalling 88215 DoF.

3.3. Simulations of the guidance force experiment

The guidance force experiment is simulated with the following goals: to compute the guidance force at different vertical positions between the guideway and the DCLCs with lateral movement of $\pm$10 mm; to observe the current density normalised by the critical current density in each tape at different time instants. This is done for the lowest height case, 20 mm, where the losses are most extreme. These analyses are essential to assess the bearing's performance during curved paths.

For all simulations, in the beginning, the guideway is 50 mm apart from the DCLCs vertically and centred horizontally. Then, the guideway moves upwards, with a speed of 1 mm/s, until a chosen height is reached. After the vertical movement is completed, the guideway moves sideways with the same speed, first 10 mm to the right, then 20 mm to the left, ending the simulation in the centred horizontal position. Three heights are investigated: 40 mm, 30 mm and 20 mm, which means 10 mm, 20 mm and 30 mm vertical displacements.

The movement is computed in the same way as in the levitation force simulations. As there is no experimental data for the guidance force so far, there is no way to verify if the 2D approximation factor for the guidance force is the same as γ. So, for this case, the guidance force density per unit length is computed

$$F_x = -\int_C B_y J_z L dC \tag{9}$$

where B_y is the magnetic induction component to the $\hat{y}$ direction.

The degrees of freedom (DoF) are the same ones from the levitation force case.

4. Results and discussions

In this section, the levitation force and guidance force tests simulation results are presented and analysed.

4.1. Model validation and levitation force results

As it was explained in the previous section, model validation is done by comparing the simulation results and experimental data collected in [5] for the $\pm$30 mm case. This means that the guideway moves upward 30 mm, then moves downward 30 mm. Fig. 4 shows the comparison of the levitation force by relative position between the guideway and the DCLCs. The simulation shows good agreement with the experimental data. For most time steps, the absolute error between the two curves fell under 5 N, around 1.77% of the maximum force. The highest differences between the simulation and the experiments are within positions 30 mm and 20 mm during the upward movement, and within 20 mm and 50 mm during the downward movement. The region between 30 mm and 20 mm during upward movement corresponds to the linear growth part of the levitation force curve. The absolute error in this region is 7.5 N or 2.65% of the maximum force. The region between 20 mm and 50 mm during downward movement is where the absolute error peaks at 20 N, around 7% of the maximum force. The simulations slightly underrepresent the absolute value of the levitation force in the upward movement between 30 mm and 20 mm distances and overrepresent it during downward movement. At the maximum force, the error is around 4 N.

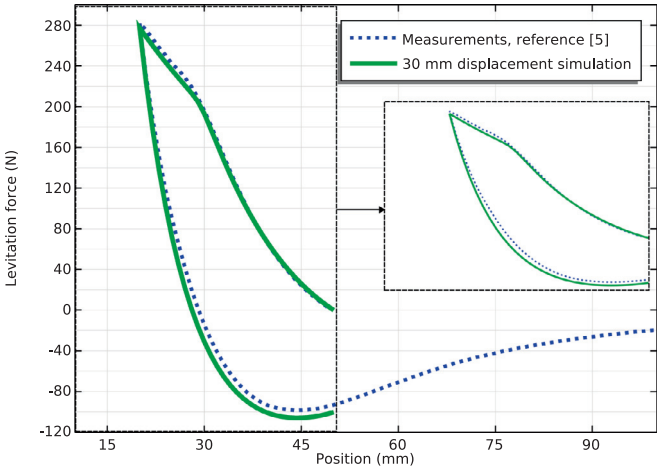

Fig. 4. Comparison of computed versus measured levitation force of the $\pm$30 mm case.

To fully understand why that happens, it is interesting to observe the local behaviour of the current density throughout the movement. This is shown in Fig. 5, where the current density normalised by local and instantaneous J_c is presented at several instants.

At the beginning of the movement, at 0 s, no current density has been induced. Then, as movement upward happens, the current density is induced, occupying the coated conductor parts from the outermost ones towards the innermost ones, see instant 15 s. At 30 s, the guideway and the DCLCs are 20 mm close, the lowest distance between them during this test. This is the point where the whole DCLC stacks are occupied with $\pm J_c$, leading to a high resistive state.

Then the magnetic field is trapped. At t = 30 s, the motion direction is reversed: the guideway starts moving downward. At instant 45 s, one can see that the current direction has been reversed at the outermost segments because the movement direction is reversed. Such reversion shields the field variation at the innermost segments, resulting in part of the current induced during upward movement still persisting. This counter-movement current decays as the DCLC and the guideway vertical distance increases, and the persistent current induced during the overall movement is present at the end of the experiment, at 60 s.

From the analysis of Fig. 5, due to the resistive state, one can see that there are high losses from the 30 mm position upward until the end of the experiment, which are also the positions where one can see the highest differences between simulations and experiments. This indicates that the simulations underrepresent the loss state. Future works should include an improved $\mathbf{E}(\mathbf{J})$ model to reduce these differences.

Fig. 6 shows the levitation force against the position results for various displacements, starting from $\pm$10 mm until the $\pm$30 mm case. One can see that from the $\pm$10 mm case to the $\pm$20 mm case, the levitation force has the banana shape one can expect for a bulk superconductor levitating over a magnetic guideway, such as the ones investigated in [12,14]. This type of curve does not present the linear region observed in the $\pm$25 mm and $\pm$30 mm cases.

This observation indicates that, for the application of stacks of coated conductors to magnetic levitation, there is a limit for the behaviour of the levitation force directly related to the high losses state. This is probably linked to the number and the material of coated conductors; and the magnitude of the magnetic field and its spread across the guideway.

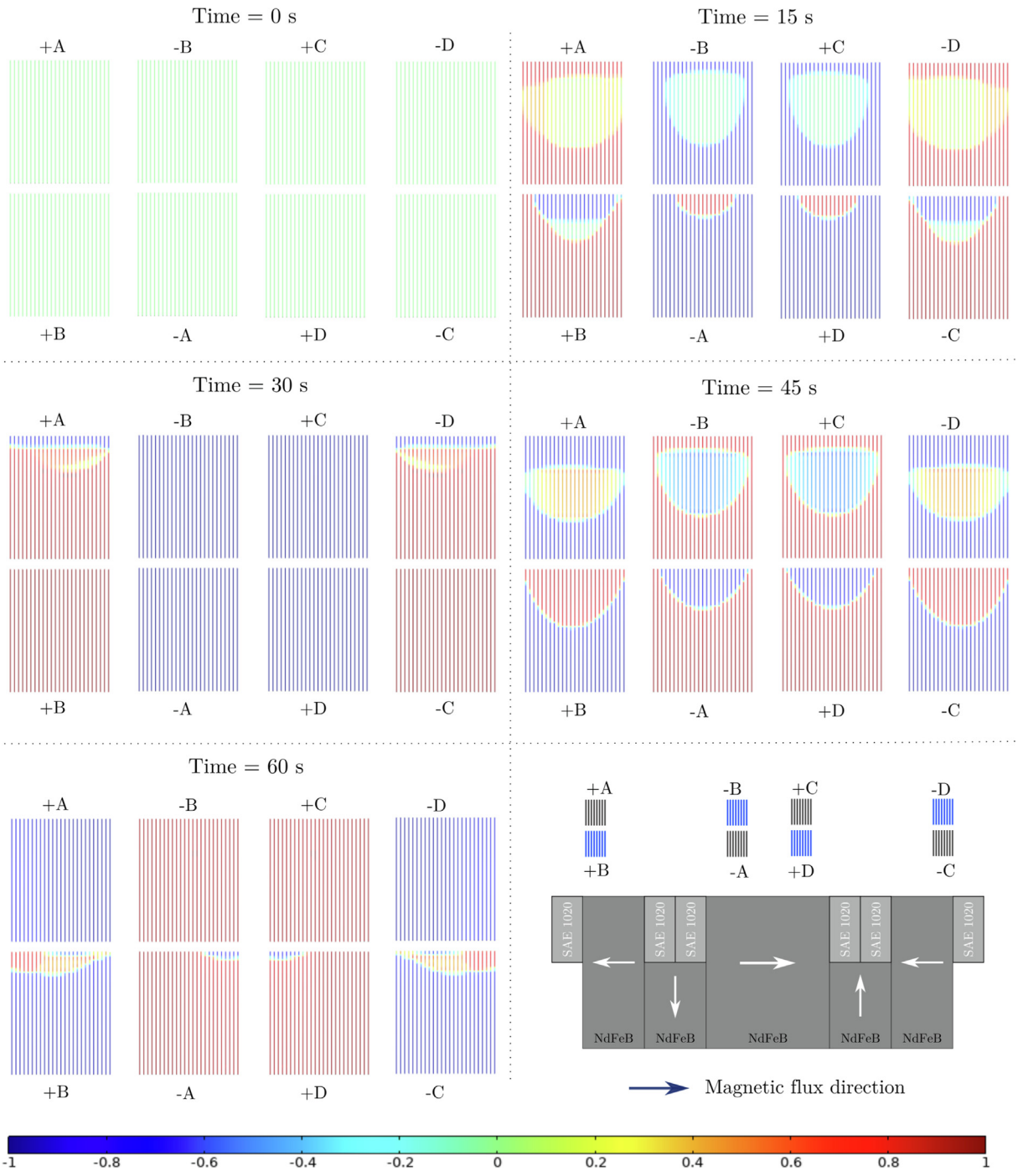

Fig. 5. Current density normalised by local J_c while the vertical distance between DCLCs and guideway changes.

The number of coated conductors controls the possible total induced current: the higher this number is, the higher the possible induced current will be. This increases the levitation force limit, as the force depends on the induced current density. The type of coated conductor material influences the losses, as it changes the quality of the pinning capacity of the superconductor. Improvement on the quality of the pinning increases J_c, which will increase the non-linear flux creep region of the E-J curve, increasing the levitation force limit.

The magnitude of the magnetic field acts on the coated conductors reducing J_c, which means that the higher the magnetic field, the lower the levitation force limit will be. And the magnetic field spread across the guideway influences its ability to induce current on the DCLCs. A study of the best magnetic field configurations for DCLCs needs to be performed so that their relationship to the levitation force for DCLCs is correctly addressed. It is included in the future works proposed in the conclusion section.

All these aspects are in line with the results and analysis found in [11,15], comparing the force developed by stacks and loops of coated conductors, and bulks, when interacting with an external magnetic field. Stacks and loops have in general more hysteresis than bulks when subjected to the same varying magnetic field, while having the best force to volume ratio.

To end the analysis of the levitation force of DCLCs, one may observe that the hysteresis of the levitation force also increases with

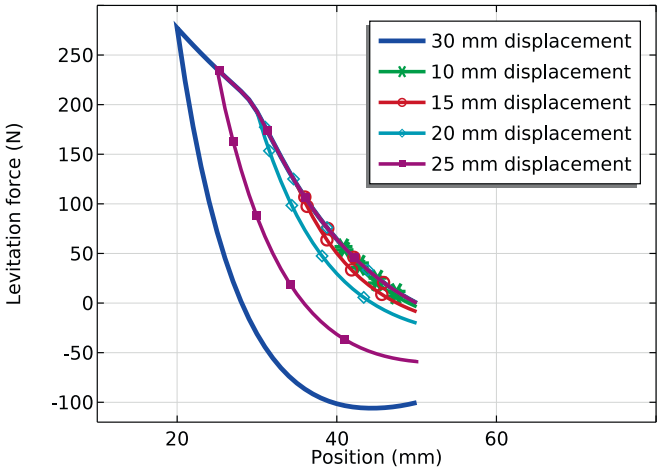

Fig. 6. Comparison of levitation force with different vertical displacements.

the overall displacement. This effect is non-linear, as one may notice by checking the levitation force at the 50 mm position after all movement is concluded. The absolute value of the levitation force almost doubles between the ±25 mm case and the ±30 mm case.

This is related to the persistent current trapped in the DCLCs after the movement. In [16], da Cruz et al. investigate the voltage behaviour of jointless loops with different states of operation: no losses, low losses and high losses. It was observed in [16] that the high loss scenario is the one that generates the highest persistent currents in the loops. This effect may explain why the lasting levitation force was much higher for the case with the highest losses, the ±30 mm case.

4.2. Guidance force analysis

With the simulation model validated as a 2D representation of the DCLCs above a magnetic guideway, the study can be extended to include the investigation of the guidance force for this type of magnetic bearing.

The analysis begins with the observation of the guidance force along the lateral displacement for three cases, identified by the height (vertical distance between guideway and DCLCs). All cases had a lateral displacement of ±10 mm, as explained in Section 3.3. Fig. 7 summarises the results. One can observe that both the magnitude and hysteresis behaviour of the lateral force density is influenced by the

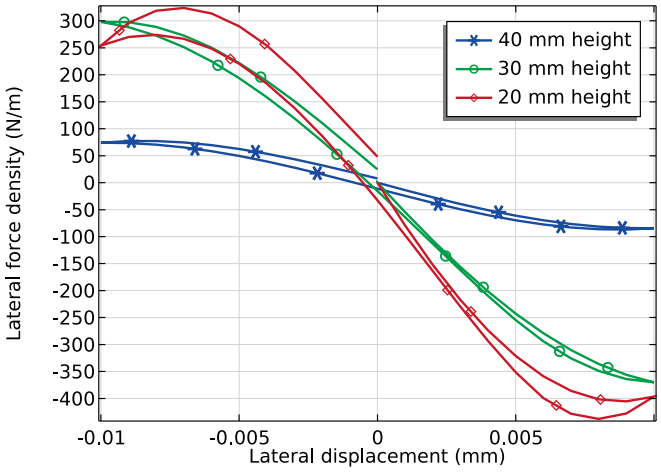

Fig. 7. Comparison of lateral force density developed during lateral movement at different heights.

vertical displacement before the lateral displacement. The 40 mm height scenario, where the vertical displacement is 10 mm, is the one with the lowest lateral force and the lowest hysteresis, having almost linear behaviour.

The 30 mm height case, with a vertical displacement of 20 mm, is the medium case, and the 20 mm height, vertical displacement of 30 mm, is the case with the highest lateral force density and highest hysteresis. For the 40 mm and 30 mm height scenarios, the maximum lateral force density occurs at the maximum lateral displacement of ±10 mm positions. For the 20 mm height, the maximum lateral force occurs at around 7 mm and 8 mm position for the right and left lateral displacements, respectively. This effect indicates how the hysteresis of the levitation force, discussed in Section 4.1, is linked to the lateral force hysteresis.

To check this effect and better understand it, it is interesting to observe the current density behaviour for various time instants for the 40 mm and the 20 mm height cases. They are summarised in Figs. 8 and 9, which show the current density normalised by local and instantaneous J_c at various time instants along the lateral movement.

Fig. 8 starts at 10 s, when the vertical movement stops for the 40 mm height scenario. There is a current circulating in the DCLCs, which was induced during the vertical movement. It can be observed that there are areas in the DCLCs without any current present. This contrasts heavily with the situation for the 20 mm height case, in Fig. 9, where, at the start at 30 s, there is induced current occupying all regions of all coated conductors.

Throughout the rest of the movement, for all lateral positions, the initial condition for lateral displacement influences the current induction behaviour. For the 40 mm case, the space not occupied by current at the beginning means there is a low loss initial condition. This leads to a low loss current induction process that culminates in a last position, at 50 s, with almost all current density flowing in a single direction for each macro region of each DCLC and with the existence of areas with no current circulating, even after all lateral movement.

The same is not true for the 20 mm case, Fig. 9. The high loss initial condition leads to high losses during all lateral movement, with all areas of the DCLCs occupied with circulating current at all time instants. This indicates and reinforces the effects observed in the levitation force analysis: that the force densities hysteresis is linked to the high loss state and the persistent current induction process.

5. Conclusion

This work provides a simulation study of a superconducting magnetic bearing with jointless loops arranged as double crossed loops made with the T-A formulation in a 2D approximation. As a 2D approximation, the jointless loops are represented as lines. An auxiliary circuit is used to couple the two parts of every jointless loop. Every part of every loop enters the circuit by its voltage drop, computed by the average of the full electric field along those lines, with contributions of the coated conductor resistivity and of the electric field induced by magnetic induction. Movement is implemented by a moving mesh configuration. The model is validated by comparison with levitation force measurements taken in [5]. Both levitation force effects and guidance force effects are investigated.

Five different vertical displacements are applied to the analysis of levitation force: ±10 mm, ±15 mm, ±20 mm, ±25 mm and ±30 mm, this last case being the one used for validation. It is shown that, for the first three cases, the levitation force behaves in the same way as it does in bulk superconductors, with a banana-like shape when plotted against position. For the last two cases, a change in levitation force growth pattern emerges, and it becomes near linear after a specific position. It is identified that there is a limit in the levitation force linked to the losses that occur with the movement. The normalised cur-

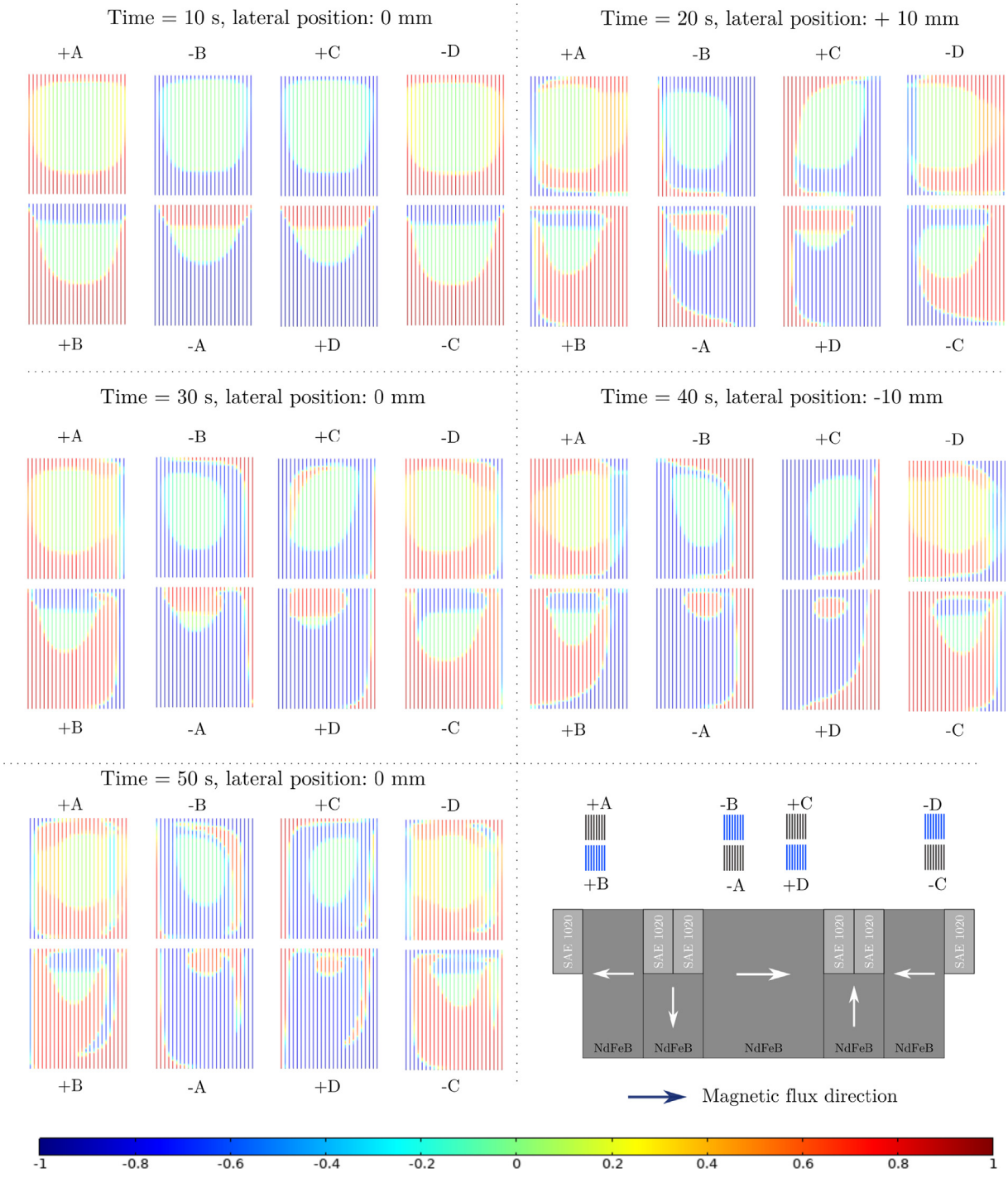

Fig. 8. Current density normalised by local J_c while the lateral distance between DCLCs and guideway changes at 40 mm height.

rent density for numerous time instants is also shown and indicates the full occupation of the loops by currents during the high loss state.

The guidance force is investigated by the observation of the guidance force density emerging from a ±10 mm horizontal displacement at three heights: 40 mm, 30 mm and 20 mm. It is shown that the hysteresis in the lateral force is linked to the hysteresis in the levitation force. Lateral force density and hysteresis increase with increasing vertical proximity between guideway and double crossed loops. Normalised current density at various time instants for the 40 mm and 20 mm are shown and compared. It is observed that the occupation of the DCLCs by induced currents at the beginning of the lateral movement is important for the overall development of the lateral force, with the 40 mm being the one where currents occupy the DCLCs the least.

Future works on this subject should include more experimental data of the levitation force; the experimental data of the lateral force, which has not been investigated as far as our knowledge goes; the investigation of the best configuration of magnetic guideway for DCLCs; and a study of the relationship between the number of tapes, the superconductor characteristics and guideway configurations to both levitation and guidance forces.

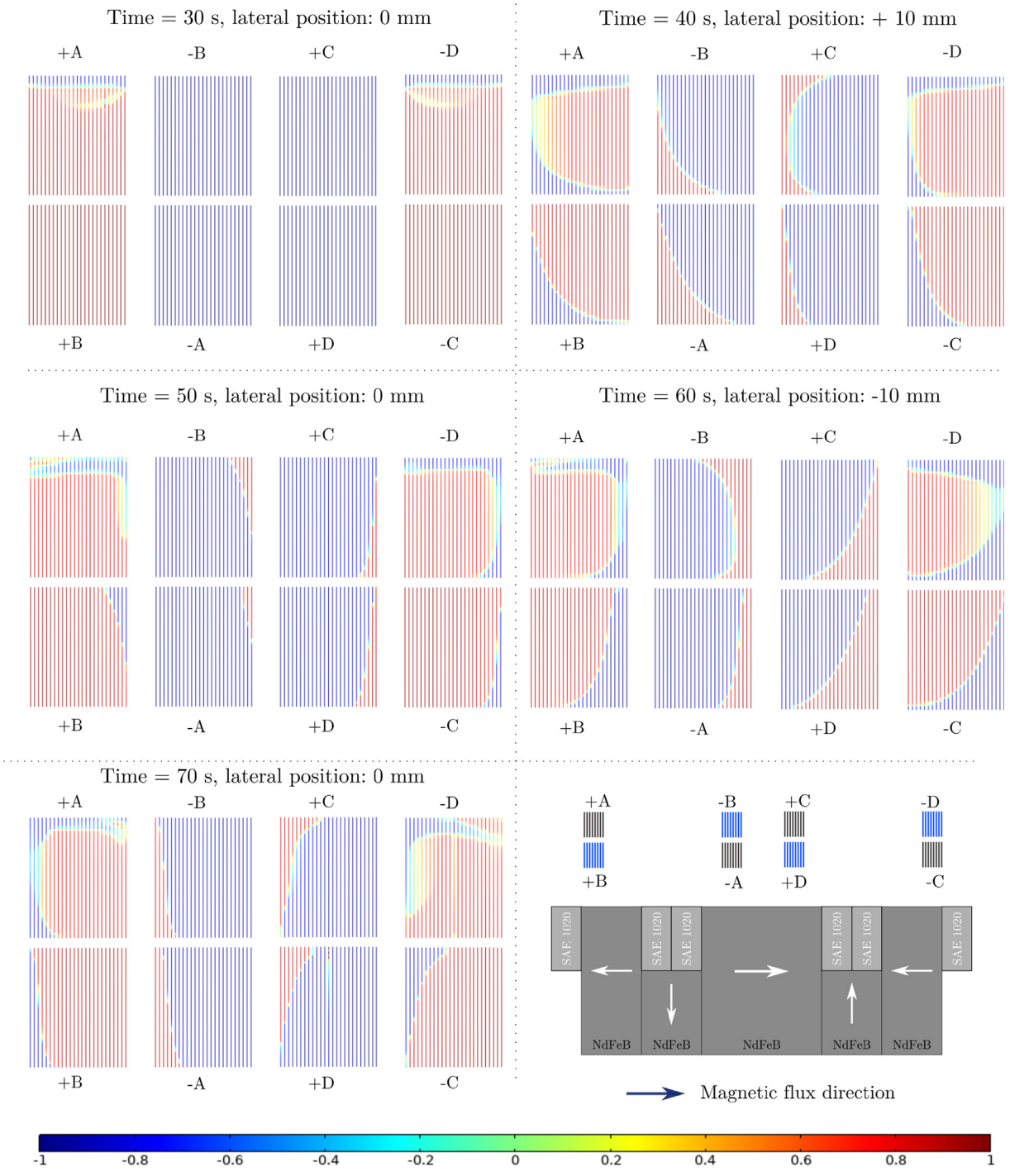

Fig. 9. Current density normalised by local J_c while the lateral distance between DCLCs and guideway changes at 20 mm height.

Declaration of Competing Interest

The authors declare that they have no known competing financial interests or personal relationships that could have appeared to influence the work reported in this paper.

Acknowledgements

This work was financed in part by the Conselho Nacional de Desenvolvimento Científico e Tecnológico - Brasil (CNPq) and by the Coordenação de Aperfeiçoamento de Pessoal de Nível Superior - Brasil (CAPES), finance code 001, INCT-CNPq INERGE and FAPERJ.

References

[1] Yazdani-Asrami M, Zhang M, Yuan W. Challenges for developing high temperature superconducting ring magnets for rotating electric machine applications in future electric aircrafts. J Magn Magn Mater 2021;522:167543. https://doi.org/10.1016/j.jmmm.2020.167543.

[2] Martins FGR, Sass F, Ferreira AC, de Andrade R. A novel magnetic bearing using rebco double crossed loop coils. IEEE Trans Appl Supercond 2018;28(4):1–5. https://doi.org/10.1109/TASC.2018.2813371.

[3] Lee H-G, Kim J-G, Lee S-W, Kim W-S, Lee S-W, Choi K-D, et al. Design and fabrication of permanent mode magnet by using coated conductor. Phys C:

Supercond Appl 2006;445–448:1099–102. proceedings of the 18th International Symposium on Superconductivity (ISS 2005). doi: 10.1016/j.physc.2006.05.044. https://doi.org/10.1016/j.physc.2006.05.044.
[4] Ali MZ, Zheng J, Huber F, Zhang Z, Yuan W, Zhang M. 4.6 t generated by a high-temperature superconducting ring magnet. Supercond Sci Technol 2020;33 (4):04LT01. https://doi.org/10.1088/1361-6668/ab794a.
[5] Martins FGR, Sass F, de Andrade R. Simulations of REBCO tape jointless double crossed loop coils with an integral equations method. Supercond Sci Technol 2019;32(4):044002. https://doi.org/10.1088/1361-6668/aafd08.
[6] Huber F, Song W, Zhang M, Grilli F. The t-a formulation: an efficient approach to model the macroscopic electromagnetic behaviour of hts coated conductor applications. Supercond Sci Technol 2022;35(4):043003. https://doi.org/10.1088/1361-6668/ac5163.
[7] Yang Y, Yong H, Zhang X, Zhou Y. Numerical simulation of superconducting generator based on the t–a formulation. IEEE Trans Appl Supercond 2020;30 (8):1–11. https://doi.org/10.1109/TASC.2020.3005503.
[8] Wang S, Yong H, Zhou Y. Calculations of the AC losses in superconducting cables and coils: Neumann boundary conditions of the t–a formulation. Supercond Sci Technol 2022;35(6):065013. https://doi.org/10.1088/1361-6668/ac6a52.
[9] Wang Y, Zheng J, Zhu Z, Zhang M, Yuan W. Quench behavior of high-temperature superconductor (RE)ba2cu3o x CORC cable. J Phys D: Appl Phys 2019;52 (34):345303. https://doi.org/10.1088/1361-6463/ab1e2c.
[10] Santos BMO, dos Santos G, Sirois F, Brambilla R, Junior RdA, Sass F, et al. 2-d modeling of hts coils with *t-a* formulation: How to handle different coupling scenarios. IEEE Trans Appl Supercond 2022;32(5):1–4. https://doi.org/10.1109/TASC.2022.3160512.
[11] Sass F, Ramos de Castro A, Gonçalves Sotelo G, de Andrade R. Persistent currents in a magnetic bearing with coated conductors. J Appl Phys 2015;118(20):203901. https://doi.org/10.1063/1.4936178.
[12] Dias DHN, Motta ES, Sotelo GG, de Andrade R. Experimental validation of field cooling simulations for linear superconducting magnetic bearings. Supercond Sci Technol 2010;23(7):075013. https://doi.org/10.1088/0953-2048/23/7/075013.
[13] Benkel T, Lao M, Liu Y, Pardo E, Wolfstädter S, Reis T, et al. T–a-formulation to model electrical machines with hts coated conductor coils. IEEE Trans Appl Supercond 2020;30(6):1–7. https://doi.org/10.1109/TASC.2020.2968950.
[14] Dias DHN, Sotelo GG, Moysés LA, Telles LGT, Bernstein P, Kenfaui D, et al. Application of textured ybco bulks with artificial holes for superconducting magnetic bearing. Supercond Sci Technol 2015;28(7):075005. https://doi.org/10.1088/0953-2048/28/7/075005.
[15] Sass F, Dias DHN, Sotelo GG, de Andrade Júnior R. Coated conductors for the magnetic bearing application. Phys Procedia 2012;36:1008–13. sUPERCONDUCTIVITY CENTENNIAL Conference 2011. doi: 10.1016/j.phpro.2012.06.097. https://www.sciencedirect.com/science/article/pii/S1875389212020342.
[16] da Cruz VS, Telles G, Santos BMO, Ferreira A, de Andrade R. Study of the voltage behavior of jointless superconducting 2g loops during pulse magnetization. IEEE Trans Appl Supercond 2020;30(5):1–6. https://doi.org/10.1109/TASC.2020.2968919.